DOE/ET/53088--450

DE91 000148

INSTITUTE FOR FUSION STUDIES

DOE/ET/53088-450 IFSR #450

Numerical Study of Compressible Magnetoconvection with an Open Transitional Boundary

H. Hanami and *T. Tajima*

Institute for Fusion Studies
The University of Texas at Austin
Austin, Texas 78712

August 1990

THE UNIVERSITY OF TEXAS

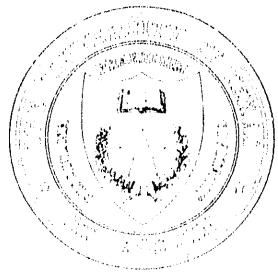

AUSTIN

Numerical Study of Compressible Magnetoconvection with an Open Transitional Boundary

H. HANAMI[a] AND T. TAJIMA
Institute for Fusion Studies
The University of Texas at Austin

Abstract

We study by computer simulation nonlinear evolution of magnetoconvection in a system with a dynamical open boundary between the convection region and corona of the sun. We study a model in which the fluid is subject to the vertical gravitation , magnetohydrodynamics (MHD), and high stratification, through an MHD code with the MacCormack-Donner cell hybrid scheme in order to well represent convective phenomena. Initially the vertical fluid flux penetrates from the convectively unstable zone at the bottom into the upper diffuse atmosphere. As the instability develops, the magnetic fields are twisted by the convection motion and the folding of magnetic fields is observed. When the magnetic pressure is comparable to the thermal pressure in the upper layer of convective zone, strong flux expulsion from the convective cell interior toward the cell boundary appears. Under appropriate conditions our simulation exhibits no shock formation incurred by the fluid convected to the photosphere, in contrast to earlier works with box boundaries. The magnetic field patterns observed are those of concentrated magnetic flux tubes, accumulation of dynamo flux near the bottom boundary, pinched flux near the downdraft region, and the surface movement

[a]permanent address; Laboratory of Physics, Iwate University, Morioka, 020 Japan.

of magnetic flux toward the downdraft region. Many of these computationally observed features are reminiscent of solar observations of the fluid and magnetic structures and their motions.

subject headings: Magnetoconvection - the Sun: convection: flux collapse

I. Introduction

On the surface of the Sun many magnetic flux tubes are observed that are confined and isolated. The presence of confined flux with strong magnetic fields was reported by many observations (continuum, Muller 1977; FeI and magnetograph, Title et al. 1987). It is likely that this magnetic structure originates from magnetohydrodynamical (MHD) effects and its motion seems to reflect that of the convection zone of the Sun. Some of the evidence are inferred from the chromosphere (H_α, Dunn and Zirker 1973; Ca, Mehltretter 1974: Mg, Spruit and Zwann 1981).

Over 90% of the magnetic flux through the solar photosphere outside sunspots is observed to be concentrated in small-scale flux tubes, which have magnetic fields 1-2kG (cf. Stenflo 1989), called kilo Gauss (kG) flux. However, the global average of the magnetic filling factor is on the order of one percent so that on the average there seem to be only weak magnetic fields, whose strength is likely to be in the range 10 -100G (Stenflo 1989). From physical considerations shown below it has been suggested that weak field magnetic flux is spontaneously concentrated into strong kG flux tubes under the influence of convective motion.

The convective instability due to superadiabatic atmosphere was pointed out by Schwarzschild (1965). This mechanism is important for energy and field transport process as in stars, including the Sun. The convective process may also be important for the formation of concentrated magnetic flux. Linear processes of the formation of magnetic tubes include the convective collapse (Spruit 1979), while nonlinear processes such as flux accumulation and amplification at convective cell boundaries may be also important. In the convection zone a vertical magnetic flux can be unstable against the convective collapse. This is incurred by the buoyancy force. This type of instability has been studied by several authors (Spruit 1979, Spruit and Zweibel 1979, Unno and Ando 1979, Moreno-Insertis and Spruit 1989, and Hasan 1984). Linear stability analysis indicates that the flux region with $\beta = 8\pi P/B^2 << 1$

is stable against the convective collapse, while one with weaker flux is unstable. Convective collapse leads to spontaneous shrinking of the magnetic region. The system then reaches a new equlibrium, in which the magnetic pressure is comparable to the external gas pressure. The pressure of 1-2 kG magnetic fields is comparable to that of the thermal pressure at the photosphere. The above scenario is thus capable of providing the possible cause of the kG flux formation.

The convective motion can also enhance magnetic fields. In ideal MHD systems frozen-in magnetic fields are carried to and accumulated at the boundaries of the convection cells (Perkins and Zweibel, 1987;Tajima and Gilden, 1987). The relationship between the flux tubes and the pattern of the convective motion has been investigated mainly with incompressible approximations (Galloway and Proctor 1983, Proctor and Weiss 1982 and Nordland 1988). They reported that isolated flux tubes can be formed at the boundary of convection cells. Studies of two-dimensional simulation for compressible magnetoconvection also exhibit the formation of concentrated flux tubes (Cattaneo 1988, Proctor 1983). They have studied systems with closed boundary conditions. There are a few works for a fully compressible system, namely by Woodward (1988), Stein et al. (1989), Nordland and Stein (1989), Cattaneo et al. (1989). In their calculations shock waves are often observed to form near the upper boundary of the box, as the fluid begins to rise, expand, and accelerate to become supersonic. The shock wave formation appears to be related to the closed boundary condition. On the surface of the Sun, however, the realistic boundary is an open one. In order to investigate the solar granulation, 3-D MHD numerical simulations with radiative heat exchange and open boundary have been carried out by Nordlund (1983, 1986). The evolution of the magnetic field in these simulations shows the convective expulsion process and no evidence of shock. Some simulations, however, use the anelastic approximation (Gilman and Glatzmaier 1981), neglecting the $\partial\rho/\partial t$ in the continuity equation, which has the effects of filtering out sound waves and cannot capture the effects related to shock waves. It is still an open question

whether the shock wave is formed or not near the photosphere in a fully compressible MHD system in an open bounadry system.

In the present paper we shall consider two-dimensional fully compressible magnetoconvection with an open boundary with many orders of magnitude of density variations. We consider an initially horizontal or vertical magnetic field and follow its linear and nonlinear evolution. We describe the basic equations, numerical method, initial conditions and boundary conditions in Sec. II. In Sec. III we show the results of our simulation. Finally in Sec. IV we discuss and make comparion of these results with the recent solar observations.

II. Equations of Magnetohydrodynamics and Numerical Method

A. Equations

Our system is described by the ideal MHD equations

$$\frac{\partial \rho}{\partial t} = -\nabla(\rho \mathbf{v}), \tag{1}$$

$$\frac{\partial \rho \mathbf{v}}{\partial t} = -\nabla \left[\rho \mathbf{v} \cdot \mathbf{v} + P\mathbf{I} + \frac{1}{4\pi}\left(\mathbf{BB} - \frac{1}{2}B^2\mathbf{I} \right) \right] + \rho \mathbf{g}, \tag{2}$$

$$\frac{\partial \mathbf{B}}{\partial t} = \nabla \times (\mathbf{v} \times \mathbf{B}), \tag{3}$$

$$\frac{\partial U}{\partial t} = -\nabla \mathbf{S} + \rho(\mathbf{g} \cdot \mathbf{v}) + \Lambda, \tag{4}$$

with the total energy U and its flux $\mathbf{S}$ defined as

$$U = \frac{\rho v^2}{2} + \frac{P}{\gamma - 1} + \frac{B^2}{8\pi}, \tag{5}$$

$$\mathbf{S} = \left(U + P + \frac{B^2}{8\pi} \right) \mathbf{v} - (\mathbf{v} \cdot \mathbf{B}) \frac{\mathbf{B}}{4\pi}, \tag{6}$$

where ρ is the mass density, $\mathbf{v}$ the velocity, P the pressure, $\mathbf{B}$ the magnetic field, $\mathbf{g}$ the gravitational acceleration, $\mathbf{AA}$ denotes a diadic tensor, and $\mathbf{I}$ is the unit tensor. As pointed

out by Deinzer et al. (1984), the variation of the adiabatic gas constant γ due to the ionization rate can be important. We treat the non-adiabatic thermal process(radiative transfer, radiative cooling and heating with MHD waves) by the term Λ, as introduced in Eq. (4). We will discuss the thermal term Λ in detail in subsection E. We allow only two-dimensional motions. The calculations are confined to the x,z plane and $v_y = 0$, $\partial/\partial y = 0$ is assumed.

B. Initial condition

The convective motion is studied in a model atmosphere, including what we may call the convective zone, the lower corona, and the "transitional" zone between the upper part of the convection region and the bottom part of the chromosphere and the photosphere. Note this "transitional" zone is not the same as the solar transition zone. These different regions are initially set in hydrostatic equilibrium under the gravity. In order to determine the initial state of this system, the vertical temperature distribution T(z) is assumed as

$$T(z) = T_0 \left(1 - \frac{(z - Z_0)}{\Delta}\right) \times \left[1 - \tanh\left(\frac{z - Z_0}{\Delta}\right)\right] + G(z) \tag{7}$$

$$G(z) = \alpha T_2 + \frac{1}{2} T_2 (1 - \alpha) \left[1 + \tanh\left(\frac{z - Z_0}{\Delta}\right)\right], \tag{8}$$

where T_0 and T_2 are the temperatures in the base of convectively unstable layer and in the corona region, respectively, Z_0 is the distance between the convective zone and the coronal zone, and Δ the scale height of the temperature in the transitional zone.

In the first example (sec.III-B), we give the profile of magnetic field $B_x(z)$ as

$$B_x(z) = \left(\frac{8\pi P(z)}{\beta(z)}\right)^{1/2}, \tag{9}$$

with

$$\beta(z) = \frac{\beta_0}{f(z)},$$

$$f(z) = \exp\left[-\left(\frac{z}{\Delta_2}\right)^2\right],$$

where β_0 is the ratio of the gas pressure to magnetic pressure at the base of the convection zone and Δ_2 is the scale height of magnetic fields. The magnetic field initially concentrates at the bottom of the convection zone. We obtain the initial distribution of density and pressure from the integration of the hydrostatic equation

$$\frac{d}{dz}\left[P + \frac{B_x^2(z)}{8\pi}\right] = -\rho g, \tag{10}$$

$$P = \rho T.$$

We can obtain the density profile from the pressure and the temperature.

We normalize Eqs. (1)-(10) as follows. The unit cell separation Δx is the unit length. The total length of the simulation box in the x and z directions is $L_x = L_z = 100\Delta x$. The unit time is determined as the free fall time t_f to traverse the vertical length of the system $100\Delta x$. Thus our gravitational acceleration is $g = 200(\Delta x/t_f^2)$. The sound speed minimum is $C_{s,min} = 12.18\gamma\Delta x/t_f$ and the sound speed at the bottom of the convection zone is $C_{s,2} = 31.6\gamma\Delta x/t_f$ such that the tempareture at the bottom is $T_2 = 1000m\Delta x^2/t_f^2 = mC_{s,2}^2/\gamma$, where m is the mass of ions or molecules and γ the gas costant. The sound transit time at the velocity minimum is $t_{tran} = (100/12.18\gamma)t_f$. We have the transitional point $Z_0 = 60\Delta x$, the scale height $\Delta = 5\Delta x$ and $\alpha = 0.01$. The initial profiles of the density and the temperature are shown in Fig. 1 for the case of a constant magnetic field or the case $\beta = \infty$, where we define $\rho = 100$ in the normalized unit at the bottom of covection zone. The profile in a finite β case is similar to this as long as $\beta >> 1$. Note that the variation of density is over many orders of magnitude; however, the variations of T and ρ are still far from the actual solar atmosphere. Here we are content with the present model resembling only qualitatively the nature of the solar variations.

C. Perturbation

A perturbation of a convective motion is imposed on the initial equilibrium. The form of the perturbation is

$$v_z = \frac{1}{\rho}\frac{\partial \phi}{\partial x}, \quad v_x = -\frac{1}{\rho}\frac{\partial \phi}{\partial z}, \qquad (0 < z < Z_s) \tag{11}$$

$$\phi = A\cos\left[\left(2\pi n\frac{z}{Z_s}\right)^{1/2}\right]\sin\left(2\pi m\frac{x}{X_{\max}}\right), \tag{12}$$

$$A = \varepsilon Z_s \rho(Z_s) C_s(Z_s), \tag{13}$$

where $\rho \mathbf{v}$ is the divergence-free density flux, Z_s the height of the top of the perturbed region, $X_{\max}$ the horizontal size of the computing domain, $C_s(Z_s)$ the sound velocity at the top of the perturbed region. A is the amplitude of the stream function ϕ, which is controlled by the parameter ε. If we take $\varepsilon < 1$ and C_s has the minimum value at Z_s, the perturbed velocity can be chosen as that of subsonic flows in all the perturbed region. We use 0.1 as the value of ε.

D. Boundary conditions

In the horizontal direction we use the periodic boundary condition; all physical values at $x = X_{\max}$ are repeated at $x = 0$. We impose the free boundary condition at the $z = Z_{\max}$ and the hard wall condition at $z = 0$, where $Z_{\max}$ is the vertical size of computing domain. We do not consider the overshooting phenomenon of the convective motion into the core and we are interested only in the upper convection zone and its immediately adjacent areas. We add the damping zone in the region $Z_{\rm up} \le z \le Z_{\max}$.

E. The treatment of the thermal process

The thermal process is complicated on the surface of the sun. In particular the transitional zone between the convection and coronal regions includes the photosphere, where the

property of energy transport by photons drastically changes. Furthermore, the temperature increases toward the corona by heating processes which have yet to be understood.

We introduce a simple (and perhaps crude) model by treating the nonadiabatic thermal process represented by Λ separate from the adiabatic part in Eq. (5) in the present calculations. We insert the following expression in each numerical time step

$$\frac{\partial T}{\partial t} = -\nu(z)\,[T - T_0(z)]\,, \tag{14}$$

where $\nu(z)$ is an empirical coefficient of the thermal process and $T_0(z)$ is the temperature profile of the assumed thermal equilibrium that is taken to be the same as the initial condition. This formula is known as the Newton approximation. The form of the coefficient is

$$\nu(z) = \nu_0 \left\{ \exp\left[-\left(\frac{(z - Z_{\rm up})}{Z_{10}} \right)^2 \right] + \exp\left[-\left(\frac{z}{Z_{10}} \right)^2 \right] \right\}, \tag{15}$$

where Z_{10} is the scale height of the thermal relaxation layers. With this empirical treatment the temperature is kept to a value close to $T_0(z)$ at the equilibrium in the transitional zone and at the bottom of the convection region. In our calculations we have the cooling effects in the transitional zone and heating effects at the bottom of the convection region. Thereby we can approximately incorporate the transport and thermal processes of the solar outer layers.

F. Numerical method

In the previous works (e.g. Graham 1975, and Hurblert, Toomre, and Massaguer 1984 without magnetic field; Hurblert and Toomre 1987 with magnetic field), in which no steep density gradient like ours was present, they used second-order-accurate numerical methods, such as the Lax-Wendroff scheme and the MacCormack scheme. These second order schemes, however, are unstable for advective motions with a steep density gradient. This is the case in our situation with the transitional zone, resulting in a break of the monotonicity of caluculated values in the system.

In astrophysical problems in which variations of physical values exist over many orders of magnitude, the flux-split scheme or second order donnor-cell scheme is often used recently (Winkler and Norman 1986). Most of these are based on the method of approximately solving characteristics of the Riemann problem in hydrodynamical systems without magnetic field. In our case, however, we must treat the advective motion of the magnetohydrodynamics including the surface of the Sun that has a steep density gradient in the transitional zone. The Riemann problem in the case with magnetic field is more complicated than that without it, because of the presence of three characteristics instead of one (simple sonic wave): the fast magnetosonic wave, the Alfvén wave, and the slow magnetosonic wave. It is, therefore, not easy to apply the method based on the Riemann problem of hydrodynamics. In calculating many astrophysical problems by the Euler scheme we face numerical problems related to the advective motion with a steep density gradient, which induces numerical instabilities (e.g. Tajima 1989). To overcome this problem, we take a type of asymmetrical finite difference scheme. The doner-cell scheme is popular in astrophysical problems. However, the original doner-cell has only first order accuracy. We need at least second order accuracy.

We use a hybrid scheme that combines the second-order MacCormack (1969) scheme with the first-order donor-cell method through a self-adjusting switch (Harten 1978). The method is hybridized through numerical fluxes in order to keep the conservative properties and the monotonicity of equations, introducing the flux mixing switch function. As the value of the switch function varies from 0 to 1, the numerical fluxes vary from the second order to first order (see Appendix A). This method starts with a higher-order method and adjusts the fluxes to give a lower-order method near the transitional zone (the steep gradient region). This scheme is related in spirit to the TVD (total variation diminishing) scheme. We checked the accuracy of this code with Alfvén wave propagation with a constant density and straight magnetic field. Further, the numerical results for an explosion problem agreed well with the Sedov-Taylor solution (Sedov 1959).

III. Results

In this section the results of our simulation are presented. We first make an introductory estimate of the stability criterion and associated time scale of convection. Then we discuss two cases:(i)convection with originally weak horizontal magnetic fields and (ii) convection with originally vertical magnetic fields.

A. Criterion of stability and characteristic time scale

We consider the criterion for the convective instability and estimate the typical time scale of this system. First, the problem of convection is examined in an unmagnetized stratified fluid (Cox 1980) with the pressure P and density ρ depending only on z as the unperturbed initial condition. Imagine a fluid element which is initially at z_0 that is displaced to a new position $z_0 + \delta z$. The density of the fluid element is in general different from that of the surrounding material. The density difference between the fluid element at the new position and the surrounding material is represented by $\Delta\rho$. The buoyancy force f_b is related to the density difference $\Delta\rho$ by

$$f_b = -g\Delta\rho = \rho g A \delta z \tag{16}$$

$$A = \left(\frac{1}{\rho}\frac{d\rho}{dz} - \frac{1}{\gamma}\frac{1}{P}\frac{dP}{dz}\right). \tag{17}$$

If f_b and δz are of the same sign, the fluid is convectively unstable. The growth rate of this instability ω_t is obtained by $\mathrm{Im}(N)$ where $f_b = -\rho N^2 \delta z$, and $N = \sqrt{-Ag}$. When $A < 0$, N is referred to as the Brunt-Väisälä frequency. The typical growth time scale of convection is $\tau \doteq 1/\sqrt{gA} = 1/\omega_t$, where ω_t is the growth rate of convective instability. With no or very weak magnetic field the convective instability sets in for $A > 0$.

In the present research, however, we need another criterion for the convective instability with magnetic fields. A sufficient condition for stability of a stratified atmosphere through

which magnetic fields wieve has been derived by Gough and Tayler (1966). Our derivation of the linear criterion of the convective instability is shown in detail in Appendix B for the case with the vertical magnetic field. Using the stellar notation of the superadiabaticity $\delta = \nabla - \nabla_a$, where ∇ is the logarithmic temperature gradient and ∇_a the adiabatic gradient, β the ratio of the gas to magnetic pressure and γ the ratio of spacific heat, the superadiabatic convective instability condition is (Appendix B)

$$\delta < 1/[1 + \gamma\beta(z)/2]. \tag{18}$$

This relation can be rewritten as

$$\left(-\frac{1}{P}\frac{dP}{dz}\right)^{-1} A \;<\; \frac{1}{[1 + \gamma\beta(z)/2]}. \tag{19}$$

The mesh size in our simulation is $\Delta z = \Delta x = 1.0$. We consider two cases. They have the same temperature structure, but different magnetic field configurations. One is with a horizontal field at the bottom of convection zone, where we have taken $\beta = 100$ at the location. The width of magnetic flux sheet is taken $\Delta_2 = 20$. Another is with a vertical field case, where we have taken various magnetic field strengths.

We chose $A \sim 0.0052\Delta x^{-1}$ at the bottom of the convection zone, and τ becomes $1.96\ t_f$, yielding the growth rate $\omega_t \sim 0.51 t_f^{-1}$. In the early linear instability phase, the convective motion grows in this time scale. During this phase magnetic fields do not dominate the fluid motion. Another important time scale τ_{th} is related to the thermal process represented in Eq. (15). This value is $\tau_{\rm th} \sim 1/\nu_0 = 0.1 t_f$. This effect is not important in the early phase, however, as long as the temperature configuration does not significantly deviate from the initial condition. When the deviation of tempareture $\Delta T = T - T_{\rm in}$ becomes as large as the value of initial temperature $T_{\rm in}$, the thermal effects play an important role and the time scale is then $\tau_{\rm th}$, as seen from Eq. (15). In the following we drop the unit to describe our computational numbers.

B. Horizontal field cases

The strength of the initial horizontal magnetic field is chosen to be so small that $\beta_0 = 100$. The initial condtions are fixed according to Eqs. (9) and (10). The effects by magnetic fields on the fluid dynamics in this case ($\beta >> 1$) is negligible. We take $\gamma = 1.1$ as the adiabatic index of the gas.

Figure 2 shows the morphology of the magnetic field vectors. The cell formation of the magnetic fields due to the convective instability can be seen. Not only the fundamental cells whose width is half the horizontal width (and approximately the height of the convection zone) but also many folded smaller cells whose width is a fraction of the fundamental convection cell are observed. This is similar to that of the Bénard problem (Chandrasekhar 1970). However, our grid is too small to resolve such important physics as the hierarchy of supergranulation, mesogranulation, and granulation. We also note that there is no signature of shocks in the upper convection zone in this run. This is in sharp contrast with the previous compressible fluid work (Cattaneo 1988, Woodward 1988), in which shocks form near the upper convection zone.

The folding of magnetic fields prominently emerges, as shown in Fig. 2(b). The domains of enhanced magnetic fields are concentrated in the boundaries of fluid convective cells. The magnetic fields are swept into the cell boundaries, as they are dragged and tucked in by the fluid motion and enhanced on the way through the dynamo effect. Notice also that the accumulation of magnetic flux near the lower boundary of the convection zone. This observed behavior of the fluid flow and magnetic flux in the convection zone is consistent with the previous works on the related subjects (Proctor and Weiss 1982; Tajima and Gilden 1987; Perkins and Zweibel 1987 ; Rosenbluth et al. 1987). In these works the authors have predicted that the cell boundaries are confined to narrow boundary regions and that $\delta_c = \Delta_c / l \sim R^{-1/2}$, where Δ_c is the width of the cell boundary, l the cell width, and R the Reynolds number or the magnetic Reynolds number. Magnetic fields are tucked mainly into

boundary layers enhanced by this concentration of flux and stretching of the fields. This flux explusion from the cell interior toward the boundary region of convection cells in this horizontal field case is similar to that with vertical fields (subsection C).

It is of interest to note that in Fig. 2 the magnetic fields pile up near the bottom boundary of the convective zone. Although there appears a small amount of magnetic flux escape into the corona, the majority stays in the convection zone. This is of interest because Kaisig et al. (1990) found that magnetic flux in an atmosphere that is even Parker (1984)-stable can be driven unstable against the buoyancy instability nonlinearly by the presence of shear flows. Their atmosphere was not superadiabatic and the convectively unstable shear flows did not exist. The present finding that the (near) lack of flux escape from the convective zone may explain the ability of stars to hold magnetic fields without quickly losing them through the Parker instability.

C. Vertical field cases

We study different cases with various initial vertical magnetic field strengths. We consider six model cases: model A, B, C, D, E, and F.

The strengths of the original vertical magnetic field B_0 are 10, 30, 50, 75, 100, 200 (β =251, 27.9, 10.0, 4.49, 2.51, and 0.628 at the bottom of the corona) for model A through F, respectively. Figure 3 shows a plot of the values of δ and $1/\left(1+\gamma\beta(z)/2\right)$ for these cases as a function of the height z. For each value of z it is convectively unstable for this plasma with vertical fields if the solid line sits above the broken one in Fig. 3. In our simulated cases most of the transitional zone ($z = 50 - 60$) does not fulfill the instability condition Eq. (19). We compare these models to illuminate the interaction of magnetic fields with the convection motion. Figures 4 and 5 are devoted to elaborate model C, while Fig. 6 covers models A, B, D, and E and Fig. 7 shows model F. In the following we shall mainly show the

overview of the results and their detailed analysis of model C as a typical example: (i) the overview; (ii) the detail structure; (iii) dependence of various magnetic strengths; and (iv) discussion of numerical diffusion. The patterns of the convective motion of models A and B are similar to this case.

1. Overview of evolution of the convection

We first describe the evolution of the magnetofluid and then discuss the structural evolution. Figure 4 shows the total magnetic, kinetic, and thermal energies as a function of time in the case of model C. They are represented by E_B, E_K, and E_{th} and are integrated in the simulation box:

$$E_B = \int \frac{B^2}{8\pi} d\mathbf{x}, \tag{20}$$

$$E_K = \frac{1}{2} \int \rho_0 {\mathbf{v}_1}^2 d\mathbf{x}, \tag{21}$$

$$E_{th} = \int \frac{P_0}{(\gamma - 1)} d\mathbf{x}. \tag{22}$$

The amplitude of the convective motion grows exponentially in time with the instability characteristic time $\tau \sim 1.96$ or growth rate $\omega_t \sim 0.51$. We can fit the growth rate of kinetic energy $E_K \propto exp(2\omega_t t)$ with $\omega_t \sim 0.51$ as shown by L_1 in Fig. 4. We may devide the evolution of the system into two phases. The amplitude of the convective motion grows first ($t \sim 3 - 10 t_f \sim 0.5 - 1.5 t_{cross}$). Then the magnetic energy increases after $t > 7 t_f \sim t_{cross}$, roughly the sound crossing time. Until $t = 7 t_f$ the magnetic field $\mathbf{B}_1$ generated from the convection motion is smaller than the initial field $\mathbf{B}_0$. In this regime $|\mathbf{B}_1| << |\mathbf{B}_0|$, we can write the induction equation(3) as

$$\frac{\partial \mathbf{B}_1}{\partial t} = \nabla \times (\mathbf{v} \times \mathbf{B}_0). \tag{23}$$

With the estimate of $\frac{\partial B_1}{\partial t} = \frac{v_1 B_0}{L}$, where L is the size of the convection cell, the velocity may be estimated with the linear instability formula as $v_1 = v_{10} \exp \omega_t t$. We obtain from Eq. (23)

$$B_1 = B_0 \left(\frac{v_{10}}{\omega_t L} \right) (\exp \omega_t t - 1) . \tag{24}$$

With Eq. (24) we can obtain approximately the time t_0 when B_1 becomes of the order of B_0

$$t_0 = \frac{ln \left(\frac{\epsilon}{\omega_t t_{cross}} \right)}{\omega_t} \sim 6.7 \sim 1.1 t_{cross}, \tag{25}$$

where we used $v_{10} \sim \epsilon C_s$ and $\frac{v_{10}}{\omega_t L} \sim \frac{\epsilon}{\omega_t t_{cross}} \sim 0.033$. We see that at this time the curve for E_B increases its slope in Fig. 4.

The approximation $B_1 \ll B_0$ breaks down and the system enters another phase when B_1 becomes of the order of B_0. In this phase, we may adopt another approximation for the induction equation $\frac{\partial B_1}{\partial t} = \frac{v_1 B_1}{L}$. As long as the energy of magnetic fields is smaller than the kinetic energy, we may estimate v_1 as $v_{10} \exp \omega_t t$. Then, we obtain

$$B_1 = B_0 \exp \left[\frac{v'_{10}}{\omega_t L} (\exp \omega_t (t - t_0) - 1) \right] , \tag{26}$$

where v'_{10} is the perturbed velocity at that time. When $\omega_t (t - t_0) \sim O(1)$, we estimate

$$B_1 = B_0 \exp \left[\frac{v'_{10}}{L} (t - t_0) \right] \sim B_0 \exp \left[0.1 (t - t_0) \right] , \tag{27}$$

where we used $v'_{10} \sim 5 \sim C_s$ at $t = t_0$ and $L \sim 50$ as a typical size of a convection cell. Using this relation, we obtain the growth of the magnetic field energy going as $E_B \propto \exp \left[0.2 (t - t_0) \right]$. We write in the theoretical growth of the magnetic energy by line L_2 in Fig. 4. Both the values of kinetic and magnetic energies are smaller than that of the thermal energy, which is represented by the horizontal dotted line in Fig. 4. The thermal energy is nearly constant and slightly decreasing in phase (d), with only $\Delta E_{th} / E_{th} \sim 0.05$.

2. Detailed structure

Figure 5 shows contours of temperature and density, velocity vectors, and magnetic field lines of model C with Figs. 5(a), (b), (c), (d) at different times. Sequences (a), (b), (c),

and (d) correspond to the temporal points marked at $t = 8.2$, 10.3, 12.4, and 16.4 in Fig. 4. The length of arrows is proportional to the absolute value of the velocity. The magnetic field structure is shown in the next panel. The evolution of the field line is controlled by the convection motion in the case of high beta $\beta = 10.0$ at the top of the convection zone. The average velocity is approximately 20 and the convection cell is symmetric as shown in sequences (c) and (d). The circumference of one convection cell is roughly 200 and the turnover time of the cell is about 10. We note, however, that since the length of the computational box is only 100 grid points, the shape of a convection cell probably strongly depends on the size of the computational box. For example, granulation cells on the solar surface have a diameter of about 1000 km. Small magnetic flux tubes have one of about 100 km. If we try to include in a realistic modelling of convection about 3 (2) convective cells and at the same time try to resolve a magnetic flux tube with about 5 grid points, we need 150 (100) grid points. We can see in Fig. 5(c) that the magnetic structure follows the winding structure of the convection cells. By the time (d) when the cell has turned over twice, magnetic field lines fold and pile up on top of each other and they are concentrated in the downdraft boundary due to the convection motion. We see magnetic field lines stretched in the horizontal direction by the motion of the material at the bottom of the convection region. In the present simulation magnetic fields at the bottom are "anchored" by the condition of a hard wall. This condition may be a reasonably close approximation of the boundary between the opaque solar core and the convection zone, although we neglect the overshooting phenomenon. Symmetry breaking of the magnetic field pattern is also observed. Even if there is originally only a vertical magnetic field, the convection generates the horizontal fields, which are swept in the bottom of the convection zone. This tendency of field accumulation near the bottom of the convection zone has been recently pointed out by many authors including DeLuca (1986) and Parker(1984). Furthermore, we see kinked fieldlines in (c) near the boundary region. This structure may be related to the magnetic convective collapse suggested (Spruit and Zweibel

1979).

3. Dependence of the magnetic field strength

In Fig. 6 we show snapshots of the magnetic structure at approximately the same time for the cases with different initial magnetic strengths. Magnetic fields not only reduce or stabilize the growth, but also modify the covection pattern. In the velocity field of model F shown in Fig. 7 (strong magnetic field case) we notice that two convection cells have split into four and become shortened in the horizontal direction when magnetic fields are strong. If magnetic fields are strong enough to resist the motion perpendicular to the field line, the fluid motion in the horizontal direction is more difficult. As seen in Fig. 6, magnetic fields are concentrated in the downflow region as the convection continues. This corroborates the solar surface observations of the convective patterns that appear in colder downdraft boundaries with concentrated flux and the sun spots (Title, Tarbel, and Topka 1987). The convective twist patterns are similar to each other; however; the models B and D of Fig. 6 show more concentration of magnetic field than that of the models A and E. We see a significant magnetic field collapse in model C. So do we in the model B and D. We observe strong magnetic flux expulsion from the interior of the cell in models B, C, and D. On the other hand, no significant magnetic flux expulsion is observed in model A. These results suggest that for magnetic fields to be expelled from the bulk of the plasma by the convection, it is necessary to have an appropriate strength of magnetic field with β of the order 10(1–100) at the top of the convective zone.

4. Numerical diffusion effects and the boundary layer

We have studied the magnetohydrodynamical system by using the finite difference method. We consider diffusion arising from numerics. We can estimate the diffusion coefficient (Appendix A) as

$$\mathcal{D} = \frac{(1-\phi)\,\Delta x|a|}{2}, \tag{28}$$

where a is the typical advective velocity. With this diffusion coefficient, we can estimate maximum saturated magnetic field $\nabla \times (\mathbf{v} \times \mathbf{B}) = \mathcal{D}\nabla^2\mathbf{B}$. As shown in Fig. 5, this typical advective velocity is mainly the velocity of fluid in the horizontal direction in the cell interior $v_z << v_x$ and $B_z >> B_x$. We thus estimate the maximum saturated field as

$$\frac{v_x B_0}{\Delta} = \mathcal{D}\frac{B_{\mathbf{max}}}{\Delta^2}, \tag{29}$$

where Δ is the scale height of the boundary layer of a convection cell. As shown in Figs. 5 and 6, most of magnetic fields are concentrated in the downdraft boundary region of convection cells. We may be able to approximate the total flux in the tube to be equal to that of the initial field in this box $B_{max}\Delta \sim B_0\Delta X$, where ΔX is the width of the convection cell in the x direction. Neglecting B_{max} by using the above relation, we rewrite the estimate, Eq. (29) as

$$\left(\frac{\Delta}{\Delta X}\right)^2 = \left(\frac{\mathcal{D}}{v_x \Delta X}\right) \sim R_m^{-1}, \tag{30}$$

where R_m is the magnetic Reynolds number. This estimation is equivalent to that of the previous works (Proctor and Weiss 1982, Rosenbluth et al. 1987). With $|a| \sim |v_x|$ and Eqs. (28) and (29), we can simplify as $\Delta^2 \sim \Delta x \Delta X$. In the present case $\Delta x = 1$ and $\Delta X = 100$, and then $\Delta \sim 10$. This estimation is in good agreement with the numerical results in the cases of models B, C, and D. However, even if model A satisfies the condition for convective instability, we cannot find the flux tube whose scale height is $\sim \Delta$ unlike other cases. This discrepancy suggests that the approximations used for the above estimation of the width of boundary region is not suitable for very weak magnetic field cases. We used

$B_z >> B_x$ to obtain Eq. (30) in the above discussions. However, if the collapsed flux tube is disturbed by the small eddies of the convection near the upper region, the fluid motion tangles with magnetic fields and the strength of B_x becomes on the order of B_z. If $B_{max}^2/8\pi > P_s$, concentrated flux tubes are no more disturbed by the convective motion in the surface region, where P_s is the pressure of the transitional zone. Stable flux expulsion needs the condtion $B_{max}^2/8\pi > P_s$. From this we can estimate the critical value of B_0 for stable flux expulsion without strong disturbance.

The relation between the initial magnetic field strength B_0 and that of the concentrated flux B_{max} and the condition $B_{max}^2/8\pi \sim P_s$ lead to an approximate expression

$$B_0 = B_{max}\Delta/\Delta x = (8\pi P_s)^{1/2}\Delta/\Delta x \sim 16, \tag{31}$$

where the value B_0 is the critical value for stable flux expulsion. The strength of the initial magnetic field of model A is smaller than the above critical value. The magnetic flux tube is disturbed even if flux expulsion occurs in model A. We see the disturbed structure at the surface in Fig. 6A. This consideration entails that significant convective flux expulsion needs a low β region above the convectively unstable region as in models B and C. In real situations, the low β region can be the corona or the chromosphere of the Sun.

IV. Summary and Discussion

We have carried out computer simulation of magnetoconvection of a compressible fluid with an open boundary under a constant gravitational acceleration and a simplified radiation function. In our simulations the pressure varies over many orders of magnitude. We summarize our results from our simulations.

1. As convective instability commences and continues, the convective motion helps stretch and fold the initial horizontal or vertical magnetic field and generates horizontal (or vertical) magnetic fields at the bottom of the convection zone, as seen in Figs. 2 and 5. Strong magnetic fields are swept into the boundary regions. Particularly they concentrate near the boundary layer of the convective zone. This result may be compared with the observation by Title et al. (1987). Their observation shows that magnetic fields are concentrated in the downflow regions due to the flows. On the other hand, magnetic fields in turn suppress the flow when they exceed a certain value in the boundary layers. There may be a considerable amount of fields at the center of granules. It seems to be related to the magnetic flux concentration in our simulation.

2. Strong vertical magnetic fields enforce the convective motion to develop primarily in the vertical direction parallel to the direction of magnetic fields, as seen in Figs. 5 and 6.

3. No shock formation is observed in our simulation of compressible, strongly stratified fluid with an open boundary, in contrast to earlier works.

4. In the downdraft region the phenomenon called the convective collapse (cf. Stenflo 1989) is observed when the beta value of the originally vertical magnetic field at the top of the convective zone is moderate $\beta \sim 1$. It is just this tendency of inhibition of convection by magnetic fields that causes the convective collapse. When β is too large, no siginificant collapse is observed. However when β is less than unity, the convective motion is largely suppressed by the fields and thus again no collapse either. The optimal β at the top of the convection zone in our run was 10 in model C.

5. The observed magnetic flux patterns are consistent with previous theory and simulation on the interaction of magnetic fields and fluid flow under the convective instability (e.g. Proctor and Weiss 1982). This behavior is one of likely mechanisms that makes the

solar magnetic flux spatially highly localized (Stenflo 1989) and everywhere else it is nearly non-existent. Our simulation shows such intermittent prerence of magnetic fields.

6. Earlier works such as Woodward (1988) and Cattaneo (1988) show shock formation particulaly in the updraft regions. Our present simulation does not. The main difference seems to stem from our adoption of the open coronal boundary. Our simulation seems more consistent with observation: Updraft flows are subsonic and no observational evidence shows shocks associated with the updraft.

7. Our observation of the concentration of flux near the lower boundary of the simulation box, which corresponds to the boundary between the convection zone and the solar core, is consistent with recent contention that the magnetic fields are generated at bottom of the convection zone (DeLuca 1987; Parker 1984). This may not be also inconsistent with the recent helioseismic observations (Leibacher et al. 1985). This is in contrast to the case where the atmosphere is convectively stable and Parker-stable but with two-dimensional shear flows (Kaisig et al. 1990): In the latter case magnetic flux may be nonlinearly driven out by the presence of shear flows, although the feet of flux tubes may be anchored. If the large magnetic structures we see in our simulation are in fact related to sun spots, it is possible that sun spots affect the solar interior.

Many important effects are still absent in the present investigation. Among the problems are 3-D effects, Coliorlis effects, the relatively small size of the computational box, and the relative simplicity of the transitional region. These are left to the future for improvements.

Acknowlegements

The work was supported by the National Science Foundation Grant ATM88-11128, Japan Society for the Promotion of Science, the Nukazawa Memorial Foundation, and U.S. Depart-

ment of Energy grant DE-FG05-80ET53088. Discussions with Dr. F. Cattaneo, Dr. G. Glatzmaier, Dr. M. Kaisig, Dr. K. Shibata, and Dr. T. Tarbell are appreciated. Professor J. Stenflo's detailed examination and suggestions have significantly clarified the paper. One of the authors (H. H.) thanks Prof. T. Nakano, Prof. S. Sakashita, and Prof. H. Sato for continuous encouragement.

References

Cattaneo, F., Chiueh, T. and Hughes, D. W., 1989, preprint.

Cattaneo, F. 1988, private communication.

Chandrasekhar, S., 1970, "Hydrodynamic and Hydramagnetic Stability," (Dover, New York).

Cox,J.P., 1980, "Theory of Stellar Pulsation", (Princeton University Press, Princeton).

Deinzer, W., Hensler, G., Schüssler, M., Weisshaar, E., 1984, Astron. Astrophys. **139**, 426.

DeLuca, E.E., 1986, Univ. Colorado, Ph.D. thesis.

Dunn, R.B., and Zirker, J.B., 1973, Solar Phys. **33**, 281.

Galloway, D.J., Proctor, M.R.E. and Weiss, N.O., 1978, J. Fluid Mech. **87**, 243.

Gilman, P.A. and Glatzmaier, G. A., 1981, Ap. J. Suppl., **45**, 335.

Gough, D.O and Tayler, R.J., 1966, M.N.R.A.S.,**133**,85.

Graham, E., 1975, J. Fluid Mech., **70**, 689.

Harten, A., 1978, Math. Compt. Phys., **9**, 568.

Hasan, S.S., 1984, Ap. J. **285**, 851.

Hehltretter, J.P., 1974, Solar Phys. **38**, 43.

Hughes, D.W. and Procter, M.R.E., 1988, Ann. Rev. Fluid Mech., **20**, 187.

Hurlburt, N. E., Toomre, J., and Massguer, J. M., Ap. J. **282** p. 557 1984.

Hurlburt, N. E. and Toomre, J., 1988, Ap. J., **327**, 920.

Kaisig, M., Tajima, T., and Shibata, K., 1990 Ap. J. **358**, 698.

Leibacher, J. W., R. W. Noyes, J. Toomre, and R. K. Ulrich, 1985, Sci. Amer. **253**, (9) p. 48.

MacCormack, R.W., 1969, AIAA paper No.**69**, 354.

Meyer, E., Schmidt, H.U., and Weiss, N.O., 1977, M.N.R.A.S., **179**,741.

Moreno-Inserts, F. and Spruit, H.C., 1989, Ap. J. **342**, 1158.

Nordlund, Å., 1983, J. O. Stenflo(ed.) in "Solar and Stellar magnetic Fields:Origins and Coronal Effects," IAU Symp. **102**, 79.

Nordlund, Å., 1985, Solar Phys. **100**, 209.

Nordlund, Å., 1986, in W. Deinzer, M. Knölker, H.H.Voigt(eds.),"Small Scale Magnetic Flux Concentrations in Solar Photosphere",Vandenhoeck Ruprecht, Göttingen, 83.

Nordlund, Å. and Stein, R. F., 1989, Ap. J. **342**, L95.

Nordlund, Å. and Stein, R. F., 1990, in Proc. IAU Symp. **138** "Solar Photosphere" eds. J. Stenflo and E. Gurtovenko (AAS, Washington, 1989).

Parker, E.N., 1984, Ap. J. **281**, 839.

Perkins, F.W. and Zweibel, E., 1987, Phys. Fluid, **30**, 1079.

Proctor, M.R.E. and Weiss, N.O., 1982, Pep. Prog. Phys., **45**, 1317.

Rosenbluth, M.N., Berk, H.L., Doxas, I., and Horton, W., 1987, Phys. Fluids, **30**, 2636.

Schwarzshild, M., 1965, "Structure and Evolution of the Stars", (Dover, New York)

Sedov, 1959, Similarity and Dimensional Methods in Mechanics."

Spruit, H.C., and Zwaan, C.,1981, Solar Phys. **38**,43.

Spruit, H.C., and Zweibel, E.G., 1979, Solar Phys. **62**, 15.

Spruit, H.C., 1977, Solar Phys. **50**, 569.

Stein, R. F., Nordlund, Å., and Kuhn, J. R., 1989, in Proc. NATO ASI. "Solar and Stellar Granulation" eds. R. J. Rutten and G. Severino (Kluwer, Dordrecht).

Stenflo, J.O., 1989, Astro. Astrophys. Review, **1**, 3.

Tajima, T. and Gilden, D.L., 1987, Ap. J., **320**, 741.

Tajima,T., 1989, "Computational Plasma Physics", (Addison-Wesley, Redwood City, CA)

Tarbell, T., S. Furguson, Z. Frank, R. Shine, A. Title, K. Topka, and G. Scharmer, in Proc. IAU Symp. **138** "Solar Photosphere" eds. J. Stenflo and E. Gurtovenko (AAS, Washington, 1989).

Title, A.M., Tarbell, T.D., and Topka, K.P. 1987, Ap. J.,**317**, 892.

Unno, W. and Ando, H., 1979, Geophys. Astrophys. Fluid Dyn. **12**, 107.

Winkler, K. A. and Norman, M.L., 1986, in "Astrophysical Radiation Hydrodynamics" K.A.Winkler and M.L.Norman (eds.), (Reidel, Dordrecht)

Woodward, P. R. and D. H. Porter, 1987, Bull. Amer. Astr. Soc. **19**, 1023.

Hitoshi Hanami: Laboratory of Physics, College of Humanities and Social Science, Iwate University, Morioka, 020, Japan (bitnet: D12697@JPNKUDPC)

Toshiki Tajima: Institute for Fusion Studies, The University of Texas at Austin, Austin, Texas 78712.

Figure Captions

Figure 1; The structure of the density and the tempareture for the initial condtion in hydrostatic equilibrium. $Z_0 = 60\Delta x$ is the coronal boundary. Note the units are those defined in the text and not degree Kelvin, for example.

Figure 2; Magnetic field vectors for the horizontal weak field case of $\beta = 100$ at the original location of flux, $\gamma = 1.1$; (a) t=11, (b) t=13, (c) t=21.

Figure 3; Comparison of the δ and the value of $1/(1 + 2\gamma/\beta)$ which are functions of the height z. $\delta > 1/(1 + 2\gamma/\beta)$ is unstable against convection.

Figure 4; Evolution of the kinetic, magnetic and thermal energies in the vertical field case (model C). The thick solid line corresponds to the kinetic energy, the dotted line to the thermal energy, and the broken line to the magnetic energy. The lines L_1 and L_2 represent the exponential growth obtained from theoritical analysis. The kinetic energy scale before $t = 6.2$ is out of scale so that we add two order of magnitude in this figure.

Figure 5; The contours of the tempareture, the density and the magnetic field lines for model C ($B_0 = 50$) in the vertical field case. The snapshot figures are at the time of (a) t=8.2, (b)t=10.3, (c)t=12.4, and (d)t=16.4.

Figure 6; Magnetic field vectors. The figures corresponds to: (a) model A(t=14.1), (b) model B (t=13.1), (c) Model D (t=12.6), and (d) Model E (t=11.6).

Figure 7; Contours of the tempareture and the density for Model F (t=8.2).

Appendix A; Numerical scheme and Numerical diffusion

We used a hybrid scheme which combines a second-order MacCormack scheme(1969) with a first-order doner cell method through a self adjusting swith (Harten 1978). Consider the advection equation:

$$u_t + au_x = 0. \tag{A1}$$

where a is the advective velocity, and the subscrit t and x represents the derivative respect to t and x. We approximate this equation by upwind finite difference form of order,

$$(u_j)_t = -a \begin{cases} \frac{u_{j+1}-u_j}{\Delta x} & (a < 0) \\ \frac{u_j-u_{j-1}}{\Delta x} & (a > 0). \end{cases}$$

The upwind form can be written as (e.g., Tajima 1989):

$$(u_j)_t = -a\frac{(u_{j+1}-u_j)}{2\Delta x} + |a|\,\Delta x\frac{(u_{j+1}-2u_j+u_{j-1})}{2\Delta x^2}. \tag{A2}$$

The first order upwind scheme is expressed as a sum of the second order symmetric finite difference scheme in the first term and the artificial diffusion effect in the second term in Eq. (A2).

We rewrite Eq. (A1) with the advective flux $f = ua$ as

$$u_t + f_x = 0. \tag{A3}$$

The first order upwind form of flux f is

$$f_{j+1/2} = \frac{f(u_j)+f(u_{j+1})}{2} - |a|\frac{(u_{j+1}-u_j)}{2}. \tag{A4}$$

We have options to take which finite difference forms for Eq. (A-4) such as the doner cell scheme, Lax-Wendroff scheme, etc.

Consider additional flux g:

$$g_{j+1/2} = \phi_j\frac{|a|}{2}(u_{j+1}-u_j), \tag{A5}$$

where ϕ is the value of order unity and will be called the flux limiter function. We add the flux g to f

$$u_t + [f + g]_x = 0. \tag{A6}$$

For $\phi = 0$ this formula becomes the purely first order upwind scheme. For $\phi = 1$, on the other hand, it becomes the second order Lax-Wendroff scheme. We control the order of accuracy of spatial derivatives in partial differential equations by chosing the value of ϕ. If we use a second order scheme, we get second order accurate results. However, the numerical instabilities arise when the monotonisity of the system cannot be retained at the discontinuity such as shock and contact discontinuities. If we use the first order scheme at the numerical unstable point where second derivative is large and the second order scheme at the stable point, we may obtain stable and aproximately second order accurate results. We introduce the switch function (Harten 1978)

$$\theta_j = 1 - \phi_j = \frac{\left|\Delta^2 u_j (\Delta x)^2\right|}{\Delta x \left(|\Delta u_j| + \left|\Delta u_{j-1/2}\right|\right) + \epsilon u_j}. \tag{A7}$$

The accuracy of the scheme of (A7) is second order at $\theta \sim 0$ when the second derivative is small, but becomes first order as the second derivative becomes large.

The MacCormack scheme is basically similar to the Lax-Wendroff. We use the hybrid scheme of MacCormack and doner-cell schemes with the above flux limiter function. From (A7) we obtain a form similar to (A3), which has the numerical diffusion term:

$$\mathcal{D} = (1 - \phi)\,|a|\Delta x. \tag{A8}$$

Appendix B; Linear analysis In order to consider the convective instability in the linear phase, we derive linearized equations from Eqs. (1) to (6). We assume vertically stratified atmosphere in hydrostatic equilibrium. In the early phase, the thermal process is negligible, which is related to the heating and cooling through exchange with radiation and magnetohydrodynamical waves. From the linearized system of Eqs. (1) to (6) we obtain the equation for the perturbed velocity:

$$\rho_0 \frac{\partial^2 \mathbf{v}}{\partial t^2} = \nabla \left[\frac{P_0}{C_v} (\mathbf{v}\nabla) s_0 + C^2 \nabla (\rho_0 \mathbf{v}) \right] - \nabla (\rho_0 \mathbf{v}) \mathbf{g} + \frac{1}{4\pi} [\nabla \times \nabla \times (\mathbf{v} \times \mathbf{B}_0)] \times \mathbf{B}_0, \quad \text{(B1)}$$

where subscripts 0 represents the values in the equilibrium state, and C is the sound velocity. We assume that the form of the perturbation is $\mathbf{v}(z) \propto exp(i(\omega t + k_x x))$

$$\left[\omega^2 - \left(C^2 + {v_A}^2 \right) {k_x}^2 + {v_A}^2 \frac{\partial^2}{\partial z^2} \right] v_x + i k_x \left(g + C^2 \frac{\partial}{\partial z} \right) v_z = 0, \quad \text{(B2)}$$

$$\left[\omega^2 + \gamma g \frac{\partial}{\partial z} + C^2 \frac{\partial^2}{\partial z^2} \right] v_z + i k_x \left[(\gamma - 1) g + C^2 \frac{\partial}{\partial z} \right] v_x = 0. \quad \text{(B3)}$$

Considering the case in which the thermal pressure is greater than that of magnetic field or the horizontal wavelength of the perturbation is smaller than the vertical scale of that variation, we assume that $(C^2 + v_A^2) k_x^2 >> {v_A}^2 \frac{1}{H_z^2}$.

We look for the mode related to the flux expulsion with the convective instability. We neglect the modes with the fast wave. This approximation gives $\omega^2/k^2 << C^2 + {v_A}^2$. We obtain a simplified equation for equations from (B2) and (B3).

$$v_s^2 v_z'' + \left[\gamma g \left({v_A}^2 / {v_f}^2 \right) - C^2 \left(C^2 / v_f^2 \right) \right] v_z' + \left[\omega^2 - \left(\gamma^2 - 1 \right) \left(g^2 / {v_f}^2 \right) - C^2 g \left(1/{v_f}^2 \right)' \right] v_z = 0 \quad \text{(B4)}$$

where $v_s^2 = \frac{C^2 v_A^2}{(C^2 + v_A^2)}$ and $v_f^2 = C^2 + v_A^2$, where v_s and v_f is related to the value of the phase speed of the slow and fast modes, respectively, and primes denote the derivatives with respect to z. We can get the eigenmodes from the equation (B4) with the boundary conditions. Our

boundary condition is $v_z = 0$ at the upper and bottom of this considered layer. We obtain from Eq.(B4)

$$H^2 v_z'' + \frac{1}{(1+\gamma\beta/2)} H v_z' + \left[\frac{\omega^2 H^2}{C^2} (1+\gamma\beta/2) + \frac{1}{2}\gamma\beta/2 \left(\delta - \frac{1}{(1+\gamma\beta/2)} \right) \right] v_z = 0. \quad \text{(B5)}$$

If the coefficient of v_z has a negative value in all regions under the above boundary condition in the third term on the left-hand side of Eq. (B5), we have no solution which has non-zero value of v_z. If $\delta < 1/(1+\gamma\beta/2)$, there is no unstable solution. This condition is identical to the Gough-Tayler condition. Furthermore, Eq. (B5) can be used to estimate the maximum of the hump of the unstable eigenfunction. At maximum, $v_z' = 0$. The depth of the hump D is estimated using

$$\frac{H^2}{D^2} \sim \frac{\omega^2 H^2}{C^2} (1+\gamma\beta/2) + \frac{1}{2}\gamma\beta/2 \left(\delta - \frac{1}{(1+\gamma\beta/2)} \right) < \frac{1}{2}\beta\delta. \quad \text{(B6)}$$

From this relation, the depth of the hump in magnetic flux tubes is given by

$$D > \sqrt{\frac{2}{\gamma\beta\delta}} H. \quad \text{(B7)}$$

If the system is near the critical state determined by the Gough-Tayler condition, we have $\gamma\beta\delta \sim 1$. In a state nearly critical, we can obtain $D \sim H$. We see that unstable eigenmodes have a typical scale comparable to the initial scale height H.

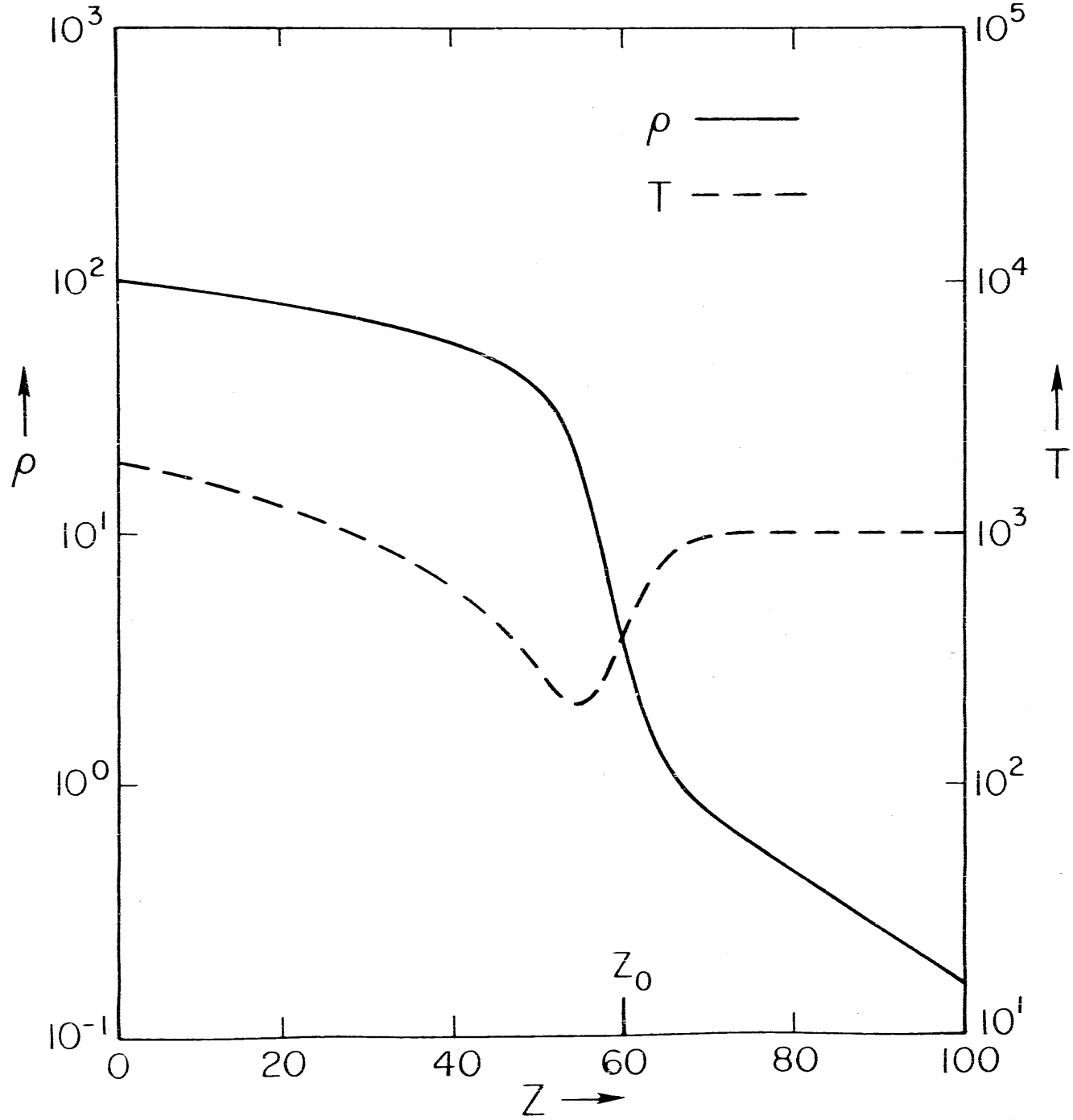

Fig. 1

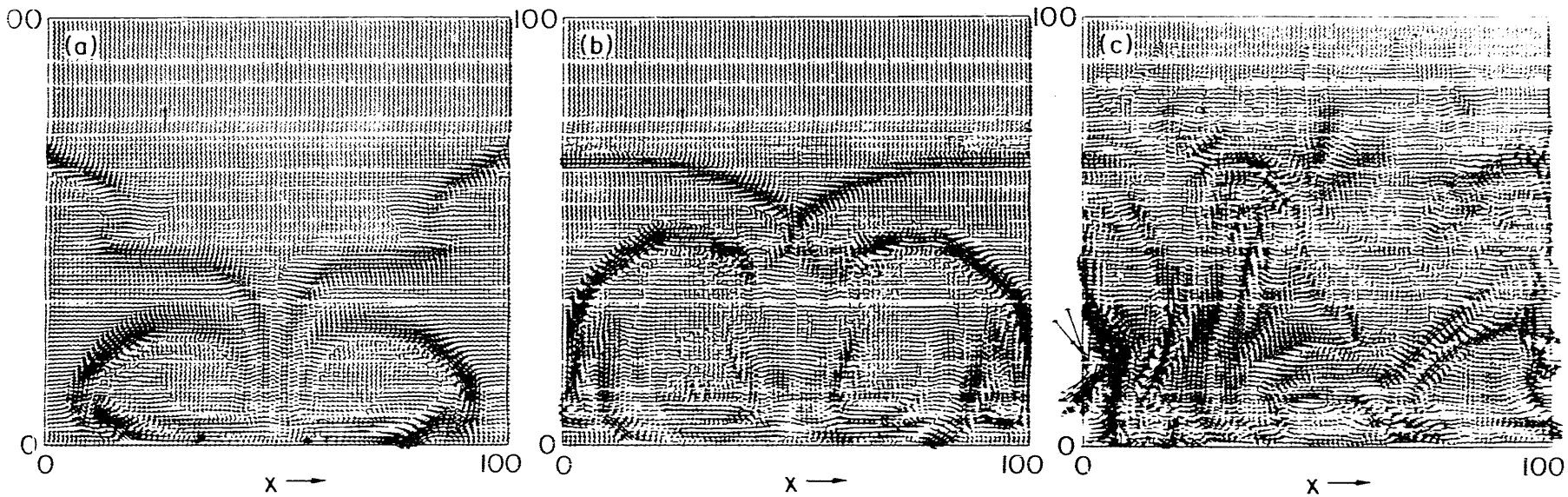

Fig. 2

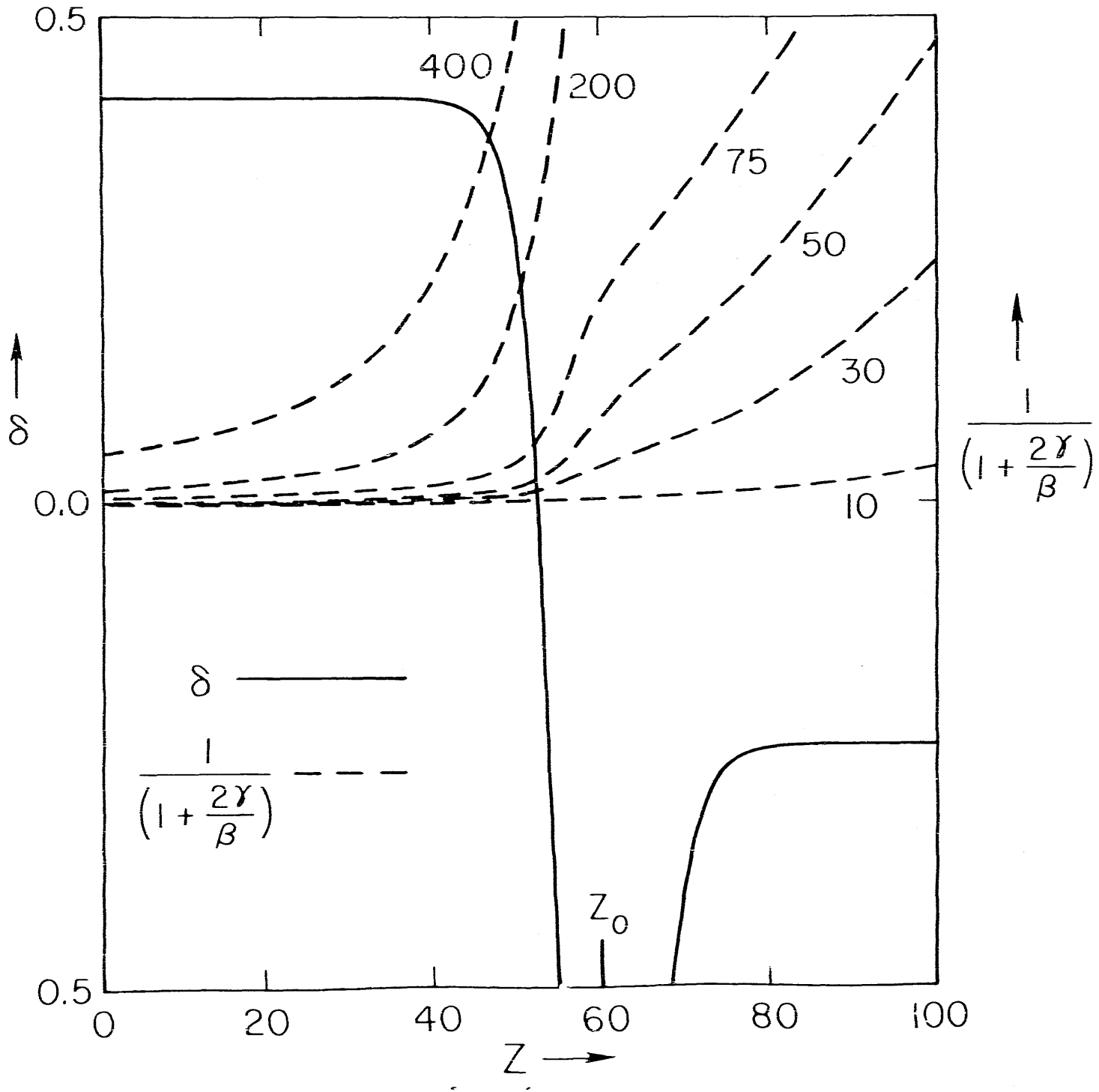
0.5
0.0
0.5
δ
400
200
75
50
30
10
$\frac{1}{(1+\frac{2\gamma}{\beta})}$
δ
$\frac{1}{(1+\frac{2\gamma}{\beta})}$
Z_0
0
20
40
60
80
100
Z

Fig. 3

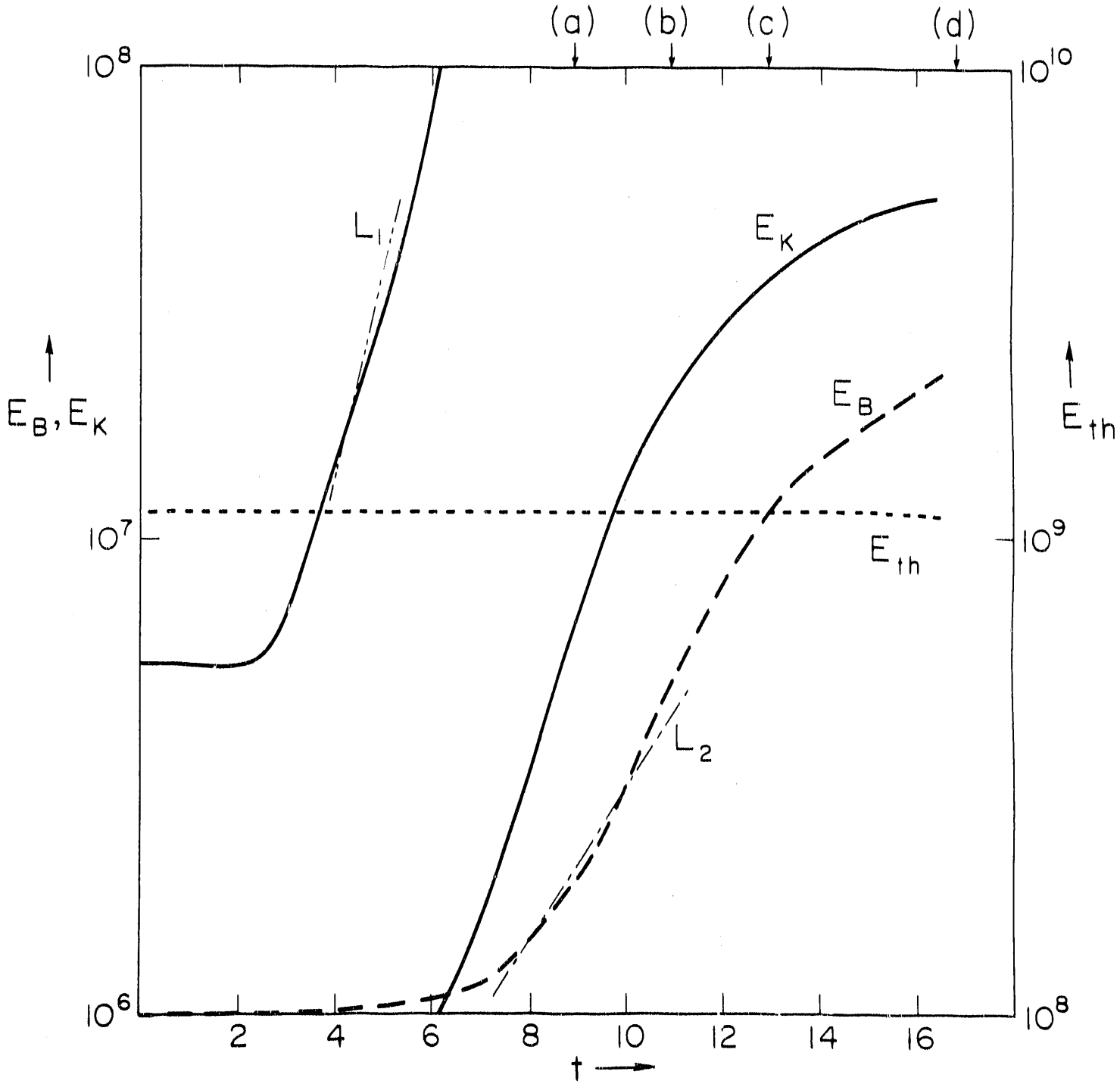
(a)
(b)
(c)
(d)
10^8
10^{10}
L_1
E_K
E_B, E_K
E_B
E_{th}
10^7
10^9
E_{th}
L_2
10^6
10^8
2
4
6
8
10
12
14
16
t

Fig. 4

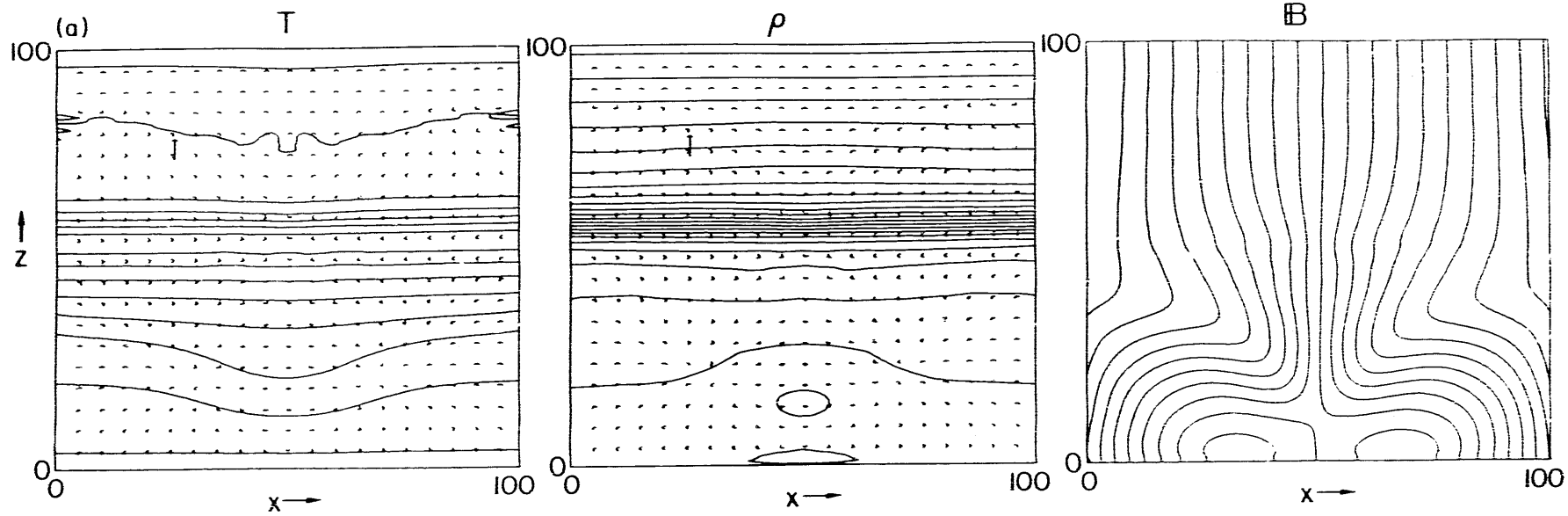

Fig. 5a

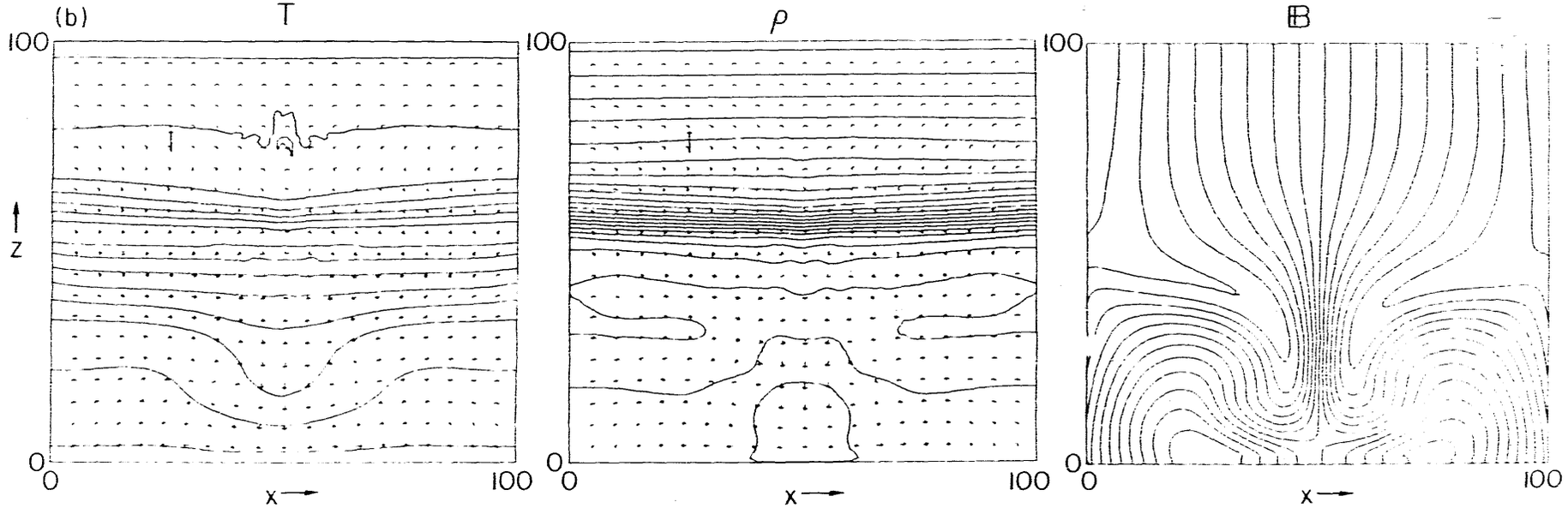

Fig. 5b

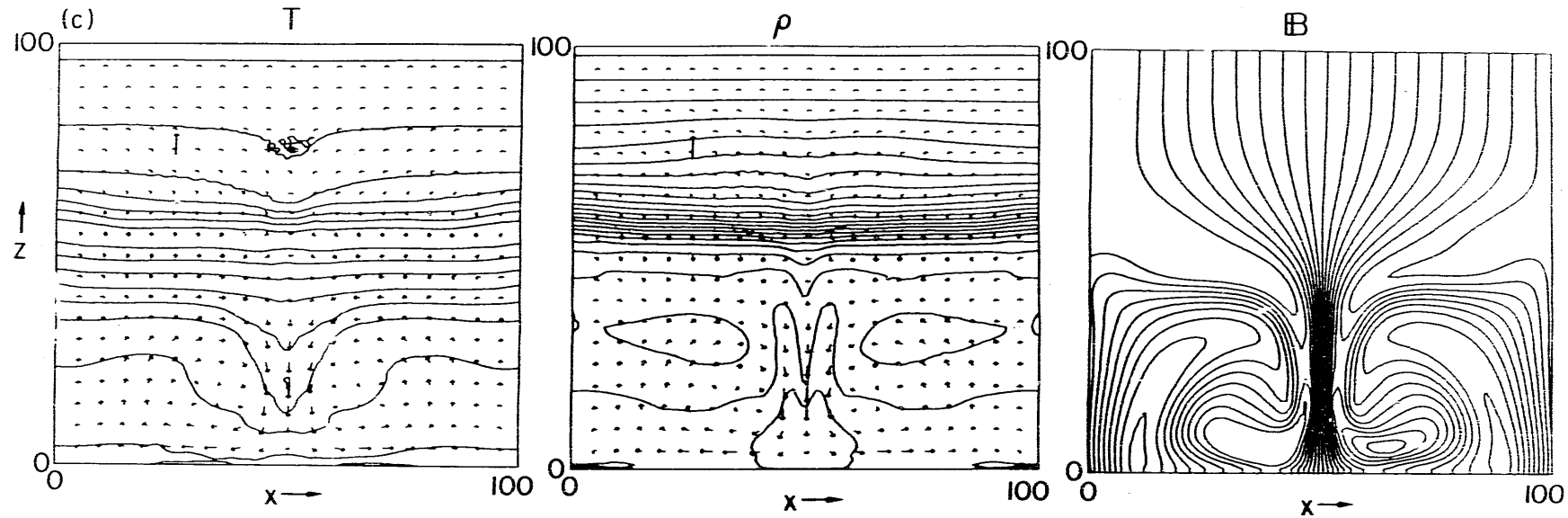

Fig. 5c

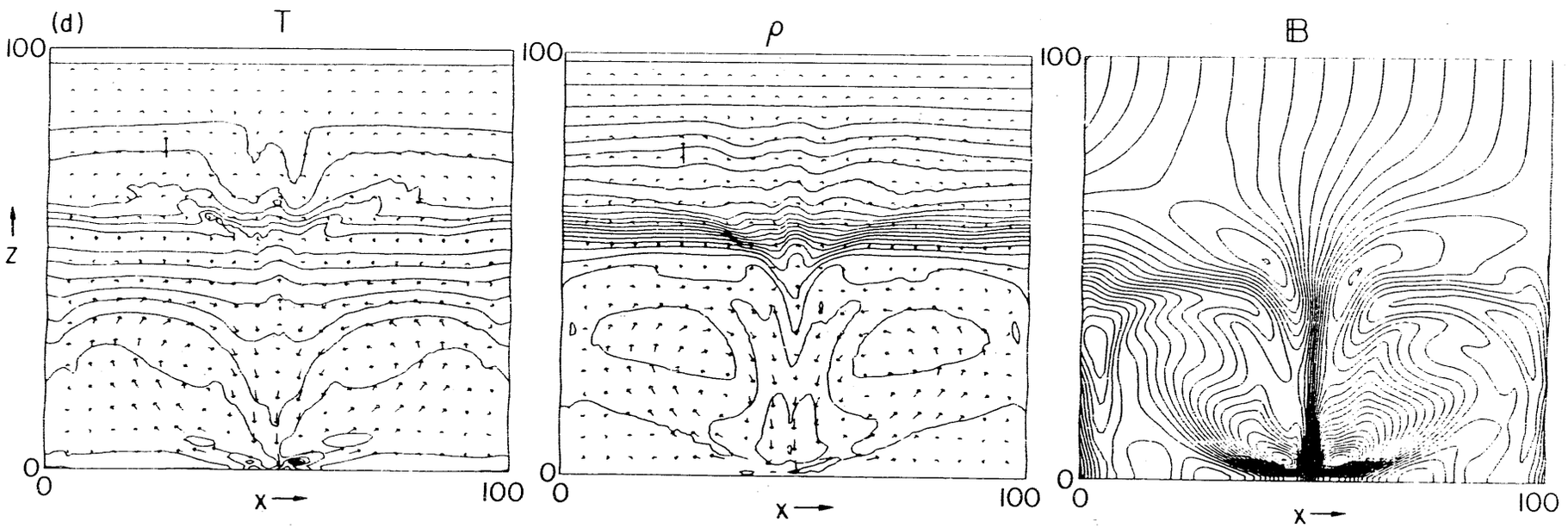

Fig. 5d

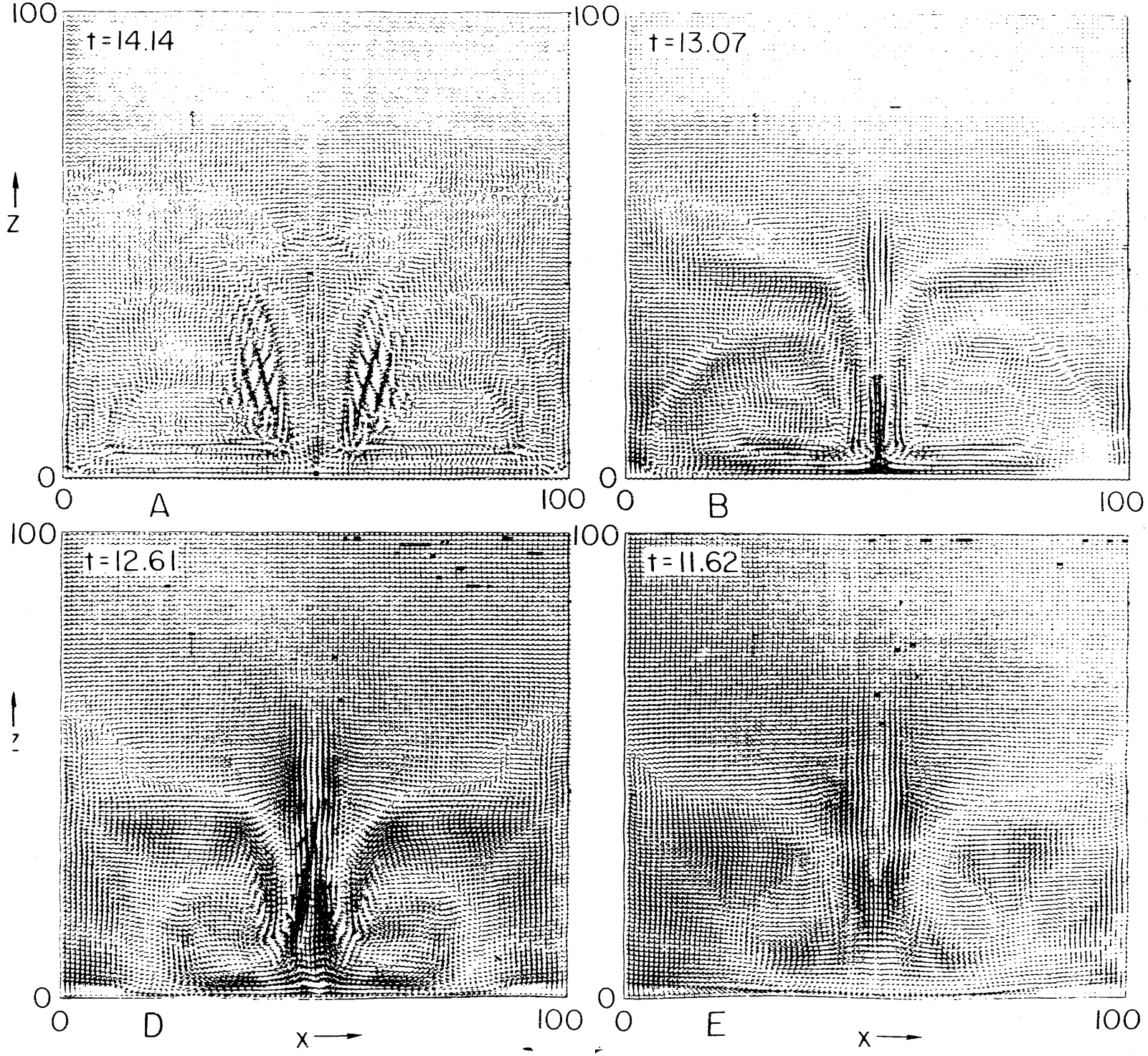
100
t = 14.14
100
t = 13.07
Z
0
0
A
100
0
0
B
100
100
t = 12.61
100
t = 11.62
Z
0
0
D
100
X
0
0
E
100
X

Fig. 6

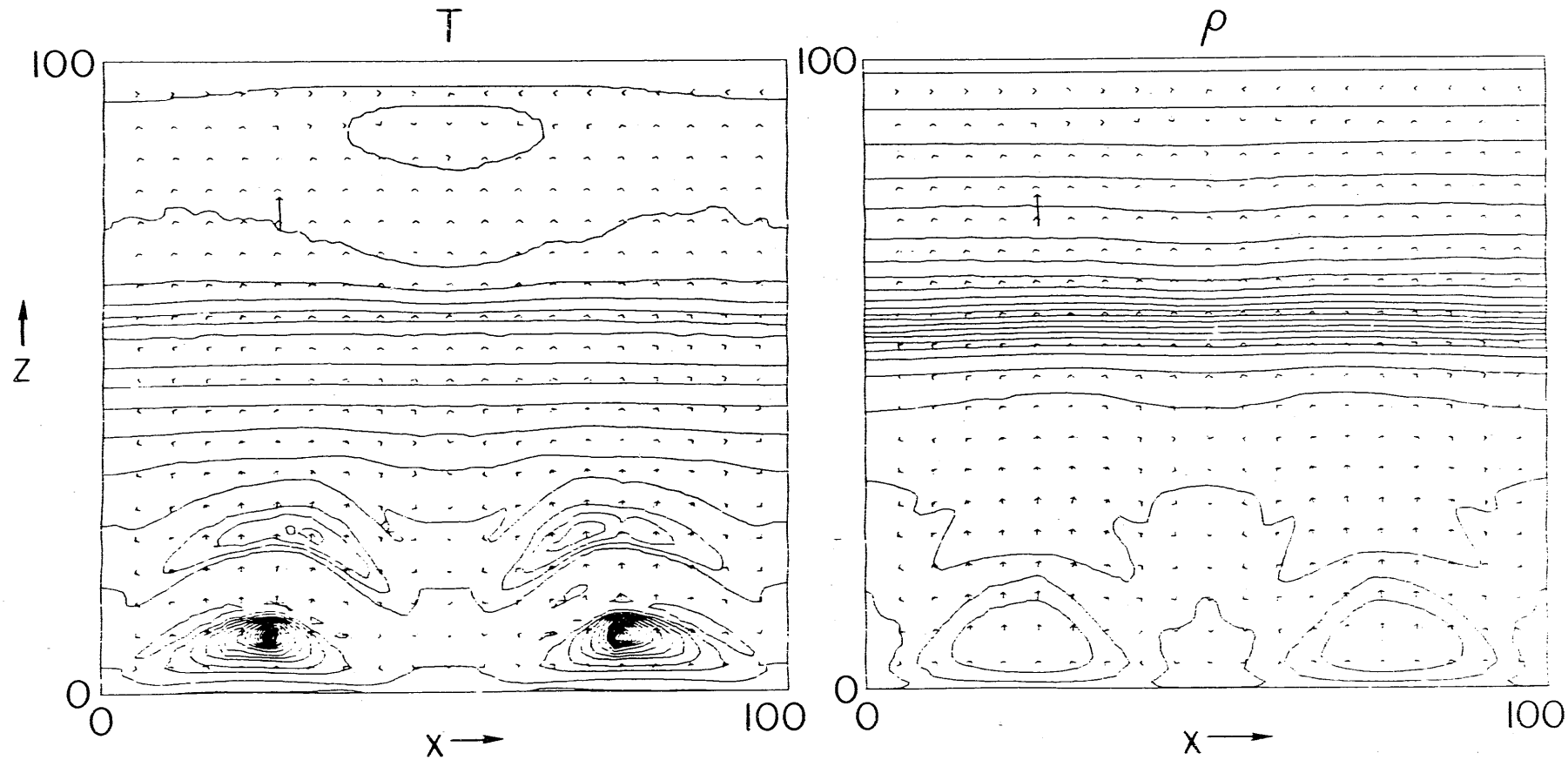

Fig. 7

END

DATE FILMED

10/16/90